JOURNAL OF PROPULSION AND POWER
Vol. 26, No. 3, May–June 2010

Film Cooling in a High-Pressure Subscale Combustion Chamber

R. Arnold,* D. I. Suslov,† and O. J. Haidn‡
DLR, German Aerospace Center, 74239 Hardthausen, Germany

DOI: 10.2514/1.47148

By the application of film cooling in addition to regenerative cooling, a considerable reduction in thermal and structural loads of rocket combustion-chamber walls can be reached. This paper discusses important influence parameters on film cooling in terms of efficiency of the injected film and wall temperature reduction. For the experimental investigations a high-pressure subscale combustion chamber operated with the cryogenic propellant combination LOX/GH_2 was used. A gaseous film with ambient tempered hydrogen was injected in the axial direction at the face plate. Typical film-cooling parameters such as film blowing rate, velocity ratio between film injection velocity and hot-gas velocity, circumferential slot positioning, and film injection slot height were investigated systematically at the European Research and Technology Test Facility P8.

Nomenclature

b	=	film-cooling slot width, mm
c_p	=	specific heat capacity for constant pressure, J/(kg K)
d	=	distance from hot-gas side, mm
l	=	lip thickness, mm
l_{rec}	=	recess length, mm
M	=	film blowing rate
$\dot{m}$	=	mass flow rate, kg/s
p	=	pressure, MPa
$\dot{q}$	=	heat flux density, W/m^2
$\dot{q}''$	=	heat flux vector, W/m^2
Re	=	Reynolds number
r	=	radius, mm
s	=	film-cooling slot height, mm
T	=	temperature, K
Tu	=	turbulence level
t	=	time, s
u	=	velocity, m/s
x	=	distance downstream of film injection, mm
γ	=	angle of film-coolant injection, °
ΔT	=	temperature error, K
$\Delta\Theta$	=	film-cooling effectiveness error
δ	=	boundary-layer thickness, mm
η	=	adiabatic film-cooling effectiveness
Θ	=	film-cooling effectiveness
λ	=	thermal conductivity, W/mK
μ	=	dynamic viscosity, kg/(ms)
ξ	=	angle in injector triangle, °
ρ	=	density, kg/m^3

Subscripts

A, B	=	hot runs
ad	=	adiabatic
cc	=	combustion chamber; hot gas
f	=	with film cooling
H_2	=	hydrogen
LOX	=	liquid oxygen
tot	=	total
W	=	wall
0	=	without film cooling
2	=	film at point of injection
1, 2	=	thermocouple number
I, II	=	slot configuration

Presented as Paper 0453 at the 47th AIAA Aerospace Sciences Meeting, Orlando, FL, 4–8 January 2009; received 11 September 2009; revision received 13 January 2010; accepted for publication 4 February 2010.

*Currently Postdoctoral Scientist, Purdue University, Department of Aeronautical and Astronautical Engineering, Maurice J. Zucrow Laboratories, 500 Allison Road, West Lafayette, IN 47907; arnold17@purdue.edu, Member AIAA.

†Research Engineer, Institute of Space Propulsion, Lampoldshausen; dmitry.suslov@dlr.de.

‡Head of Technology, Institute of Space Propulsion, Lampoldshausen; oskar.haidn@dlr.de. Member AIAA.

I. Introduction

ROCKET engines are one of the most powerful machines ever developed, featuring a thermal power of several gigawatts. To provide the enormous high power density inside a combustion chamber of a typical liquid rocket engine, highly energetic and cryogenic propellants such as liquid oxygen (LOX) and liquid hydrogen (LH_2) are used. Herewith, hot-gas temperatures $T_{cc} > 3500$ K arise with combustion-chamber pressures p_{cc} exceeding 10 MPa by far (space shuttle main engine is $p_{cc} = 19$ MPa [1], RD-0120 is $p_{cc} = 21.8$ MPa [2], and Vulcain 2 is $p_{cc} = 11.5$ MPa [3]). Because of hot-gas temperatures and combustion-chamber pressures, local wall heat flux densities $\dot{q}$ of more than 100 MW/m^2 have to be compensated by the cooling system of the engine. The throat area with a maximum wall heat flux density especially needs precise and extensive cooling efforts to survive during a hot run. A regenerative cooling system alone is insufficient in high-performance rocket engines because of pressure drop in cooling channels as well as manufacturing and structural limits [4]. A further improvement of regeneratively cooled systems could be either done with a higher velocity of the coolant in the cooling channels or by a further reduction of the wall thickness between coolant and hot gas. However, a higher coolant velocity would increase the pressure drop, resulting in additional loads for the propellant feed system. A reduced wall thickness, on the other hand, would increase manufacturing risks, since current wall thicknesses (for example, in the Vulcain 2) are already far below 1 mm, and it would also reduce safety and reliability of the combustion chamber. For higher combustion-chamber pressures and heat flux densities, regenerative cooling has to be augmented with an additional cooling system, such as film injection, to guarantee a safe operation and long duration.

In the past, a variety of different cooling systems for short- and long-duration applications were developed to guarantee a safe and steady-state temperature distribution inside the chamber wall material during a hot run [5]:

1) Ablative cooling is used especially for short-duration systems such as booster engines with a limited operating time of about two minutes.

2) Featuring the radiation-cooling method, comparatively low heat flux areas of liquid rocket engines such as nozzle extensions are cooled.

3) With dump cooling, the coolant is pouring through cooling channels inside the liner material and is dumped overboard at the end of the nozzle skirt through sonic outlets, which provides some additional thrust.

4) With regenerative cooling, the coolant flows through cooling channels, but afterwards is injected into the combustion chamber. Regenerative cooling is the standard cooling system for almost all modern main stage, booster, and upper stage engines.

5) The film-cooling method can be used either alone for comparatively low heat flux areas or in combination with regenerative cooling for very high heat flux densities.

Despite substantial progress in numerical simulation during the last years, realistic experimental data at representative enginelike conditions for further verification and development of numerical film-cooling design tools still do not exist in open literature. Although there have been only a few experimental investigations on film cooling in rocket combustion chambers, the influence of typical parameters such as blowing rate, velocity ratio, or circumferential slot positioning at real enginelike conditions on film-cooling effectiveness has been considered even less in the past [6–9].

In open literature, mostly for airbreathing application of high-pressure turbine cooling, nondimensional adiabatic effectiveness η is a widely used parameter for describing and comparing film-cooling effectiveness [10–12]. The local temperature difference between adiabatic wall temperature T_{ad} and hot-gas temperature T_{cc} is compared with the temperature difference between film-coolant injection temperature T_2 and hot-gas temperature:

$$\eta(x) = \frac{T_{\mathrm{ad}}(x) - T_{\mathrm{cc}}}{T_2 - T_{\mathrm{cc}}} \tag{1}$$

However, due to hot-gas temperatures much higher than 3400 K when using highly energetic and cryogenic propellants such as $\mathrm{LOX/H_2}$, adiabatic wall temperatures would far exceed safe operating temperatures of conventional copper materials. It is useful to establish a new local temperature ratio $\Theta(x)$ to describe film-cooling effectiveness in a convectively and film-cooled combustion chamber. The local temperature difference due to the application of film cooling will be compared with the maximal achievable temperature difference, where $T_{W,0}$ designates the wall temperature without, and $T_{W,f}$ designates the wall temperature with film cooling [13–15]:

$$\Theta(x) = \frac{T_{W,0}(x) - T_{W,f}(x)}{T_{W,0}(x) - T_2} \tag{2}$$

The temperature ratio $\Theta(x)$ can be used as a measure of the film-cooling effectiveness downstream from the point of injection at $x = 0$ within the parameters of $\Theta(x) = 0, \ldots, 1$. In the case of an agreement of the wall temperature without film cooling and the wall temperature with film cooling, $T_{W,0}(x) = T_{W,f}(x)$, the film-cooling effectiveness becomes $\Theta(x) = 0$. A wall temperature identical to the injection temperature of the film, $T_{W,f}(x) = T_2$, results in a film effectiveness $\Theta(x) = 1$.

In terms of a preferably homogenous coolant distribution in a lateral direction downstream of the slot, a continuous film injection would be the best choice. However, due to constructional limitations, this cannot be achieved in most cases. Single-injection slots will be used instead to provide the best possible coolant distribution on the chamber wall [16,17]. A detailed description of previous film-cooling investigations at DLR Lampoldshausen using a high-pressure subscale combustion chamber can be found in the literature [13–15,18].

Typical velocity and temperature profiles for tangential two-dimensional slot injection are depicted in Fig. 1. The film coolant enters at the axial position $x = 0$ via a slot (slot height s, lip thickness l) in the combustion chamber. The area downstream from the point of film-coolant injection can be divided into three major sections [19–21]:

1) Because of a clear separation of secondary flow and main flow, the effect of the film is maximal in the core zone.

2) Accompanying a mixing of film coolant into the hot-gas flow, a gradual reduction of the film-cooling efficiency with increasing distance downstream of the point of injection is the result in the mixing zone.

3) The mixing of the film coolant into the core flow is completed in the boundary-layer region. Because of a fully turbulent core flow in rocket engines, the mixing takes place very fast in comparison with other film-cooling applications.

II. Experimental Setup and Measurement Technique

All investigations presented in this paper were performed at two test campaigns (campaign A and campaign B) at the European Research and Technology Test Facility P8 at DLR Lampoldshausen. This test facility permits investigations with liquid or gaseous hydrogen at typical rocket-engine-like operating conditions [22,23].

A. Subscale Combustion Chamber E

Subscale combustion chamber E (BKE), as depicted in Fig. 2, is the newest development for high-pressure investigations at the test facility P8 [16,17,24].

Stabile operation can be guaranteed for a chamber pressure up to $p_{\mathrm{cc}} = 15$ MPa in combination with a very high mixture ratio of oxidizer to fuel (ROF). Modular design of the experimental combustion chamber ensures a maximum of flexibility for varied experiments and chamber configurations. Subscale combustion chamber E features a cylindrical segment with an overall length of 200 mm and an inner diameter of 50 mm, and a nozzle segment with a throat diameter of 33 mm. Convective cooling of both segments is provided by water that is heated by streaming through axially arranged cooling channels.

B. Film Injection Segment and Injector Head

The injector head (see Fig. 3) contains 15 coaxial injection elements arranged in two different pitch circles, with 10 elements in the outer circle, 5 in the inner circle, and a central torch igniter. The geometrical distribution is made in that way to get five identical injector triangles with one coaxial element of the inner and two elements of the outer pitch circle. Within one injector triangle, the inner coaxial element is located at $\xi = 18°$, and symmetrical boundaries of the injector triangle are at $\xi = -18$ and 54° [16–18,24].

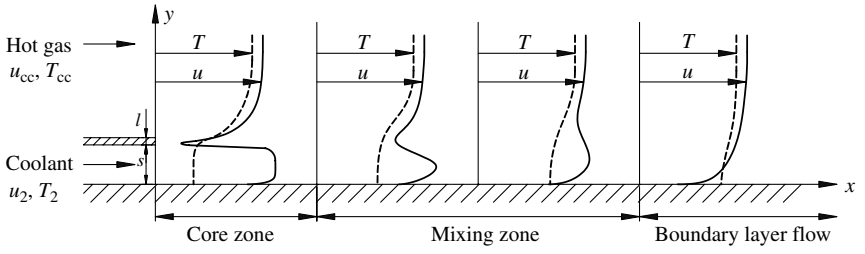

Fig. 1 Velocity and temperature profiles for tangential slot injection.

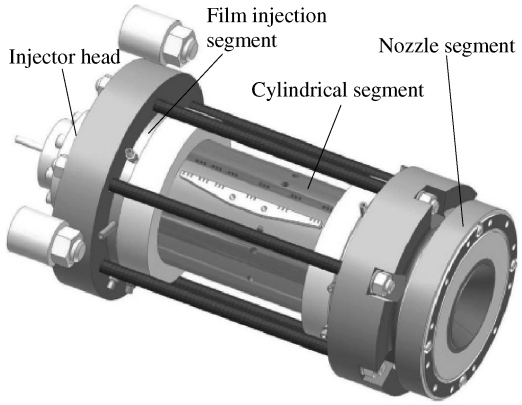

a) BKE–overview

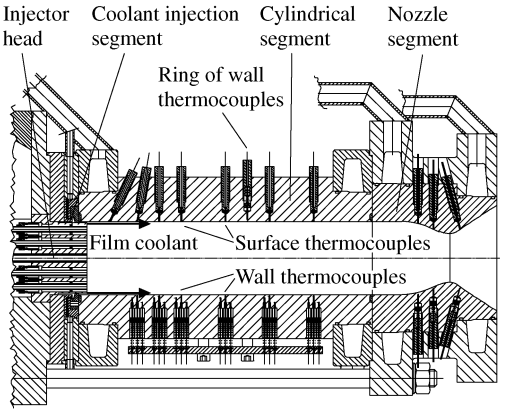

b) BKE–sectional drawing

Fig. 2 Subscale combustion chamber E.

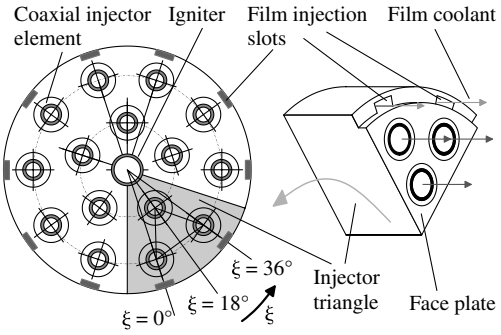

Fig. 3 Injector head and film-coolant injection segment.

Figure 4 shows the engineering design of a single coaxial injector element as well as a close-up of the leading edge of the face plate.

The recess lengths were varied within the present study. Two different recess lengths were applied: $l_{\text{rec}} = 0$ and 4 mm. Except for the investigation of the influence of the recess length in Sec. III.F, a constant recess length $l_{\text{rec}} = 0$ was used.

For film-cooling investigations, the injector-head face plate is surrounded by a coolant injection segment (see Fig. 3). This segment provides 10 cooling slots evenly distributed in a circumferential direction, manufactured with high precision for tangential ($\gamma = 0°$) film-coolant injection.

For most of the investigations, positions of these film-cooling slots were consistent with the angular positions of the outer injector elements. For each of the five identical injector triangles, the film-coolant injection slots and outer coaxial injector elements have been arranged in the angular positions $\xi = 0$ and 36°. However, for investigation of the influence of the slot positioning (see Sec. III.E), slot positions were arranged at the angular positions between the outer coaxial injector elements at $\xi = -18$, 18, and 54°.

To ensure developed two-dimensional flow characteristics of the injected coolant, a length-to-height ratio of the film-coolant slots of about $\approx$10 was arranged. Since high-precision knowledge of the injected film temperature is essential for film-cooling investigations, two thermocouples were attached in the film injection segment to measure the film temperature just before the film coolant enters the combustion chamber.

Because of the modular design, it is possible to change slot geometry and angular slot positioning of the film-coolant injection segment in a very easy way. Table 1 gives an overview of the film-cooling slot geometry.

C. Instrumentation and Measurement Technique

Subscale combustion chamber E is equipped with a multiplicity of measurement sensors for pressure, temperature, and mass flow rates. Surface and wall thermocouples are integrated in the cylindrical segment and in the nozzle segment in the subsonic part as well as in the supersonic part [14–16,18,24].

The application of surface thermocouples at different axial positions allows for the direct measurement of the local surface temperatures inside the combustion chamber, whereas wall thermocouples can only measure the wall temperatures in the chamber material at a certain distance d away from the surface. Thus, packages with three wall thermocouples each, with differing distances d ($d_1, \ldots, d_3$) from the hot-gas side are also located in axial direction inside the combustion-chamber material, as depicted in Fig. 2. An axial distance of only 1.5 mm between the thermocouples within a package ensures that the measured temperatures are nearly at the same location. From the measured thermal gradient almost perpendicular to the chamber wall, it is possible to extrapolate the surface temperature at $d = 0$ with the use of Fourier's law of heat conduction [25]:

$$\dot{q}'' = -\lambda \nabla T \tag{3}$$

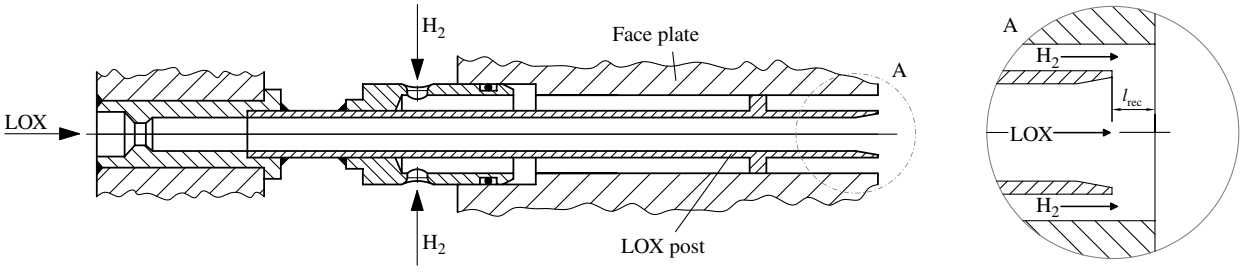

a) Design of a coaxial injector element **b) Close up of leading edge**

Fig. 4 Coaxial injector element.

Table 1 Data of the coolant injection segment

Slot number	10
Film injection angle γ, °	0
Slot height s for campaigns A and B, mm	0.40 ± 0.015
Slot height s for campaign B, mm	0.25 ± 0.015
Slot width b, mm	3.5 ± 0.015

With the assumption of a rotational-symmetry-constructed geometry, and considering a combustion-chamber radius $r = 25$ mm, the logarithmic temperature distribution as a function of the wall distance d perpendicular to the surface inside the chamber wall material can be written as (*gradient method*) [16,26,27]

$$\frac{\partial^2 T}{\partial (r+d)^2} + \frac{1}{r+d}\frac{\partial T}{\partial (r+d)} = 0 \rightarrow T(r+d) = T_{W1} + \frac{T_{W2} - T_{W1}}{\ell_n\left(\frac{r+d_2}{r+d_1}\right)} \ell_n\left(\frac{r+d}{r+d_1}\right) \tag{4}$$

By using the logarithmic temperature distribution following Eq. (4), the local wall heat flux density can be calculated as ($\lambda_W =$ 350 W/(mK) [28])

$$\dot{q} = \frac{\lambda}{r}\frac{T_{W1} - T_{W2}}{\ell_n\left(\frac{r+h_2}{r+h_1}\right)} \tag{5}$$

Because of the high heat conductivity of the chamber wall material, a uniform temperature distribution close to the hot-gas side can be assumed. The small wall distances of the thermocouples allow a precise determination of the local heat flux density and surface temperature.

Sound levels, vibrations, and thermal material expansion and contraction may cause a liftoff and loss of mechanical contact of the thermocouples. A specially designed spring system was developed at DLR Lampoldshausen to provide a constant force to ensure reliable contact during hot-run tests [26].

D. Operating Conditions

To gain detailed information about film-cooling effectiveness with a minimum of necessary hot runs and testing days, a special test sequence with a test duration of 80 s was generated. Three major pressure levels were performed: 11.5 MPa (intervals 1–3), 8 MPa (intervals 4–6), and 5 MPa (intervals 7–9), using a constant propellant mixture ratio ROF = 6 (see Table 2). Typical hot-gas parameters such as mass flow rates of injected hydrogen $\dot{m}_{H_2}$ and LOX $\dot{m}_{LOX}$ are also specified in Table 2 [24].

Each pressure interval was divided into three sections with differing film-coolant mass flow rates $\dot{m}_2$, which gave nine different operating conditions for each hot run. To give a reference in comparison with no film cooling, the last interval of each pressure step was performed without film injection ($\dot{m}_2 = 0$). Tables 3 and 4 feature a summary of film-cooling parameters such as film mass flow rate $\dot{m}_2$, injection temperature T_2, film blowing rate M (see Sec. III.A), and velocity ratios u_2/u_{cc} and u_2/u_{H_2} (see Sec. III.C) for the investigated film-coolant slot heights $s = 0.4$ mm (campaigns A and B) and $s = 0.25$ mm (campaign B). Gaseous hydrogen with ambient temperature was used as the film coolant for all tests.

III. Experimental Results

In general, film-cooling effectiveness is dependent on a multitude of geometrical (injection angle, slot height, slot width, and number of slots), fluidmechanical (blowing rate, ratios of momentum flux and boundary-layer thickness, turbulence levels, and Reynolds numbers), and thermodynamical parameters (pressure, temperature, and ratios of pressure and temperature) [9,29,30]:

$$\Theta = f\left(\frac{x}{s}, M, \frac{T_2}{T_{cc}}, \frac{u_2}{u_{cc}}, \frac{\rho_2}{\rho_{cc}}, \frac{Tu_2}{Tu_{cc}}, \gamma, \frac{c_{p,2}}{c_{p,cc}}, \frac{\mu_2}{\mu_{cc}}, \frac{\lambda_2}{\lambda_{cc}}, \frac{\delta_2}{\delta_{cc}}\right) \tag{6}$$

In addition, film cooling in a rocket combustion chamber is also influenced by injector design such as recess and tapering, LOX injection temperature, and slot positioning relative to the injector elements when considering a film injection in close proximity of the injector head.

A. Influence of Film Blowing Rate

The film blowing rate M is a main parameter to characterize film cooling. It describes the ratio of the mass velocity of the coolant to the hot-gas stream mass velocity [9]:

$$M = \frac{(\rho u)_2}{(\rho u)_{cc}} \tag{7}$$

Experimental work in the past has shown a clear connection between film blowing rate and film-cooling effectiveness for $M \leq 1$ as well as for $M > 1$ [9,31,32]. An increase of the film blowing rate M up to $M \approx 3$ indicates a better film-cooling effectiveness for tangential slot injection. This also applies for foreign gas injection in place of the well-examined case of air injected into air [9,31–33]. However, when using a film injection following inclined holes or slots, a blowing rate higher than $M = 1.5$–2 showed no further increase in film-cooling efficiency [34,35]. An inclined cooling stream with high density and high velocity can break through the hot-gas boundary layer without showing an effective cooling [36,37].

For the present investigations in the cylindrical part of subscale combustion chamber E, the influence of the film blowing rate M is clearly visible for all pressure intervals (see Fig. 5). A higher film blowing rate directly results in a more pronounced film-cooling effectiveness Θ. The impact of the coolant flow is not only noticeable in close vicinity to the film injection point ($x/s \rightarrow 0$), but also further downstream. However, for an increasing nondimensional film-cooling length x/s, differences between higher and lower film blowing rates are reduced (see Fig. 5). Because of the turbulent character of the hot-gas flow, a mixing of the coolant into the hot gas takes place with increasing film-cooling length.

Although the influence of the film blowing rate M on film-cooling effectiveness Θ is dependent on the axial distance x/s, a clear connection between film blowing rate M and film-cooling effectiveness Θ can be stated regarding Fig. 5. A linear connection between the film blowing rate and the film-cooling effectiveness can be assumed in the investigated range of parameters:

$$\Theta \propto M \tag{8}$$

B. Influence of Combustion-Chamber Pressure

Figure 6 depicts the film-cooling effectiveness Θ in the cylindrical part of the combustion chamber (see Fig. 2) downstream of the angular position $\xi = 18°$ (see Fig. 3) for the investigated pressure intervals $p_{cc} = 11.5$, 8, and 5 MPa, using a film slot height $s =$

Table 2 Hot-gas conditions

Interval	1	2	3	4	5	6	7	8	9
t, s	10–13	20–23	27–30	36–39	44–47	51–54	60–63	67–70	75–78
p_{cc}, MPa	11.94	11.84	11.62	8.29	8.16	8.02	5.15	5.07	4.97
$\dot{m}_{H_2}$, kg/s	0.60	0.60	0.60	0.42	0.42	0.42	0.26	0.26	0.26
$\dot{m}_{LOX}$, kg/s	3.62	3.61	3.61	2.51	2.51	2.51	1.58	1.58	1.58

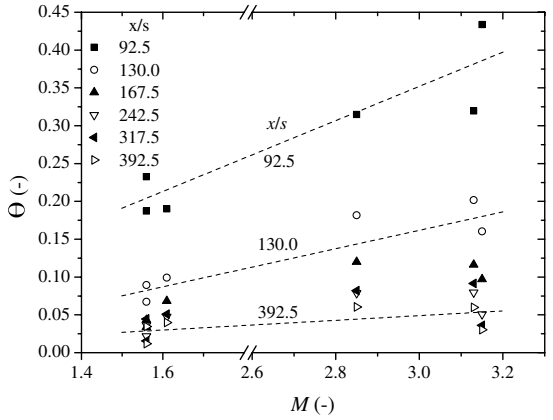

Fig. 5 Influence of blowing rate M ($\xi = 18°$).

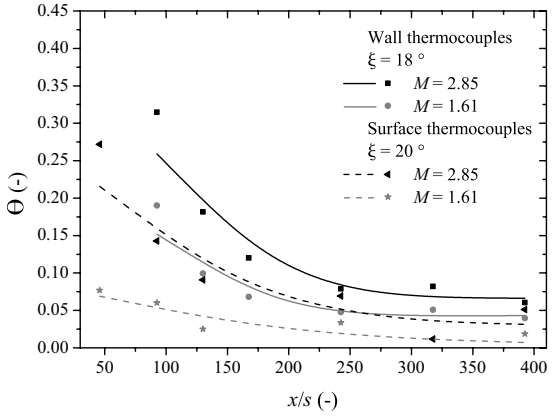

a) p_{cc} = 11.5 MPa

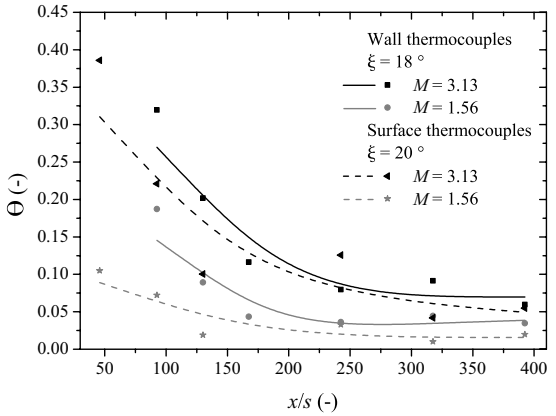

b) p_{cc} = 8 MPa

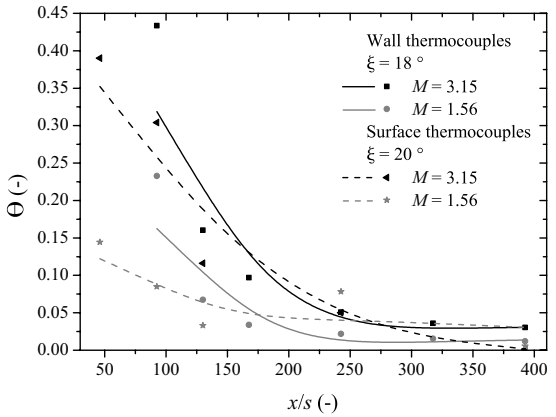

c) p_{cc} = 5 MPa

Fig. 6 Influence of film blowing rate M and combustion-chamber pressure p_{cc} ($\xi = 18°$).

0.4 mm (see Tables 2 and 3). Results of wall thermocouples located at the angular position $\xi = 18°$ agree satisfactorily with data from surface thermocouples positioned at $\xi = 20°$. To ensure an identical wall distance of $d = 0$ for both types of measurements, the gradient method [see Eq. (4)] was applied to calculate the surface temperatures from the wall thermocouple measurements. The small angular deviation between the arrangement of the surface thermocouples compared with the position of the wall thermocouples is negligible in the present study. Film-cooling effectiveness of the 11.5 and 8 MPa pressure intervals decreases similarly in the downstream direction. Maximum efficiency appears directly downstream of the point of injection, subsequently followed by the typical decay characteristics reported from different authors (e.g. [9,31,33,37,38]). However, except for the front area of the cylindrical chamber segment in close vicinity to the injector head and film injection position, film-cooling effectiveness of the lower pressure step of $p_{cc} = 5$ MPa is marginally smaller than for higher pressure steps. Although the influence of the combustion-chamber pressure on axial film-cooling effectiveness is comparatively small for the wide range of combustion-chamber pressures of 5–11.5 MPa investigated within the scope of the present study. Figure 6 also emphasizes the dominant influence of the blowing rate on film-cooling effectiveness.

C. Influence of Velocity Ratio and Slot Height

Provided that the density ratio of hot gas and injected coolant can be considered to stay constant, the film blowing rate M [see Eq. (7)] is a direct function of the velocity ratio between coolant injection velocity u_2 and hot-gas velocity u_{cc}:

$$M \propto \frac{u_2}{u_{cc}} \tag{9}$$

Film-cooling effectiveness Θ as a function of the velocity ratio u_2/u_{cc} and the slot Reynolds number Re_2 is shown in Fig. 7, in which coolant slot heights $s = 0.4$ mm (campaigns A and B) and $s = 0.25$ mm (campaign B) were distinguished for the investigated pressure intervals $p_{cc} = 11.5$, 8, and 5 MPa, respectively (see Tables 2–4). For a slot height of $s = 0.4$ mm, an increase of the velocity ratio u_2/u_{cc} results in a direct gain in film-cooling effectiveness for all investigated pressure levels (see Figs. 7a, 7c, and

Table 3 Film-cooling parameters ($s = 0.4$ mm)

Interval	1	2	3	4	5	6	7	8	9
$\dot{m}_2/\dot{m}_{tot}$, %	1.83	1.03	0	2.01	0.99	0	2.01	0.98	0
T_2, K	287.5	287.5	-	288.3	289.2	——	289.6	290.4	——
M	2.85	1.61	0	3.13	1.56	0	3.15	1.56	0
u_2/u_{cc}	1.60	0.91	0	1.74	0.87	0	1.75	0.86	0
u_2/u_{H_2}	0.94	0.52	0	1.07	0.53	0	1.08	0.53	0

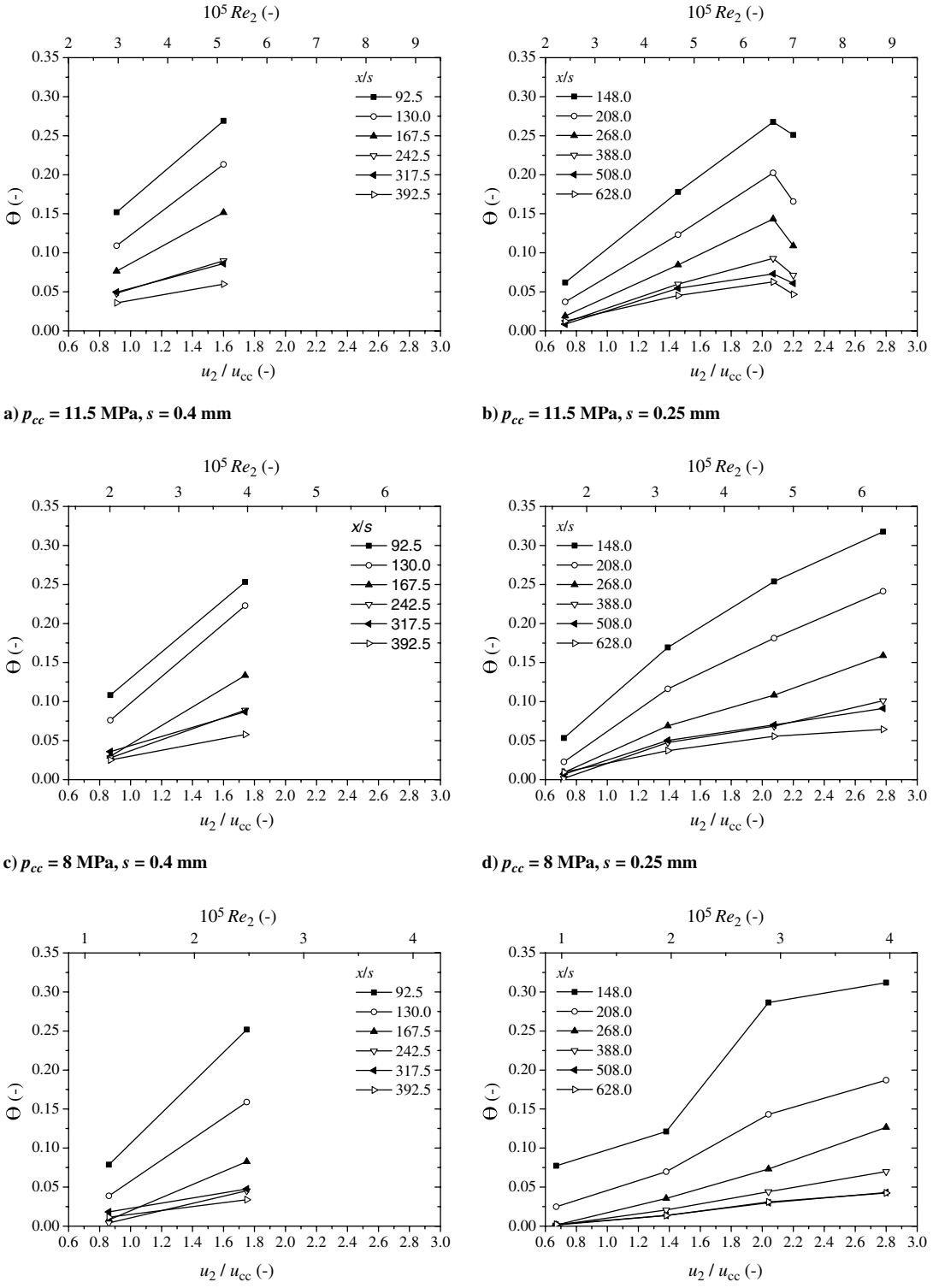

a) p_{cc} **= 11.5 MPa,** s **= 0.4 mm**

b) p_{cc} **= 11.5 MPa,** s **= 0.25 mm**

c) p_{cc} **= 8 MPa,** s **= 0.4 mm**

d) p_{cc} **= 8 MPa,** s **= 0.25 mm**

e) p_{cc} **= 5 MPa,** s **= 0.4 mm**

f) p_{cc} **= 5 MPa,** s **= 0.25 mm**

Fig. 7 Influence of velocity ratio u_2/u_{cc} and slot Reynolds number Re_2 ($\xi = 18°$).

7e). Downstream of the point of injection, the influence of the velocity ratio is more pronounced for small film-cooling lengths $x/s = 92.5$–130.0, whereas for an increased distance ($x/s > 242.5$) the influence of the velocity ratio on film-cooling effectiveness decreases considerably.

Investigations with a reduced slot height $s = 0.25$ mm showed a similar connection between film-cooling effectiveness and velocity ratio (see Figs. 7b, 7d, and 7f) for the pressure intervals 11.5, 8, and 5 MPa, respectively. However, a slight flattening of the effectiveness increase can be reported for very high slot Reynolds numbers Re_2. For the 5 and 8 MPa pressure steps (see Figs. 7f and 7d), the flattening of the increase of the film-cooling effectiveness starts at $Re_2 \approx 3\times 10^5$. Because of high turbulence levels and shear effects between film and hot-gas stream at very high slot Reynolds numbers $Re_2 > 6.5 \times 10^5$, resulting in a faster mixing of the coolant into the main stream, a reduction of the film-cooling effectiveness can be detected in Fig. 7b for the 11.5 MPa pressure interval.

With the assumption of a linear connection between single measurement points of film-cooling effectiveness Θ and velocity ratio u_2/u_{cc} in Fig. 7, Fig. 8 displays the correlation between film

Table 4 Film-cooling parameters ($s = 0.25$ mm

Interval	1	2	3	4	5	6	7	8	9
$\dot{m}_2/\dot{m}_{tot}$, %	1.49	0.50	0	1.50	0.51	0	1.47	0.49	0
T_2, K	288.4	288.4	——	288.6	288.9	——	289.3	290.1	——
M	3.68	1.29	0	3.72	1.29	0	3.68	1.21	0
u_2/u_{cc}	2.07	0.73	0	2.08	0.72	0	2.04	0.67	0
u_2/u_{H_2}	1.21	0.43	0	1.27	0.44	0	1.26	0.41	0
$\dot{m}_2/\dot{m}_{tot}$, %	1.59	0.99	0	2.00	0.99	0	2.01	0.99	0
T_2, K	287.7	287.8	——	288.9	290.2	——	290.4	290.6	——
M	3.91	2.58	0	4.99	2.49	0	5.05	2.49	0
u_2/u_{cc}	2.20	1.46	0	2.78	1.39	0	2.81	1.38	0
u_2/u_{H_2}	1.29	0.85	0	1.71	0.84	0	1.73	0.84	0

effectiveness Θ and film-cooling length x/s for a velocity ratio $u_2/u_{cc} = 1.4$. As a result, it may be stated that the local film-cooling effectiveness $\Theta(x/s)$ depends in the first instance on the velocity ratio and slot Reynolds number, respectively. Results of the upper pressure steps 11.5 and 8 MPa clarify this for a wide range of nondimensional film-cooling lengths $x/s = 92.5$–628. For a small film-cooling length not too far downstream of the injector-head face plate and film-coolant injection slots, the film-cooling effectiveness of the 11.5 MPa pressure step (see Fig. 8a) shows higher values compared with the lower pressure step (see Fig. 8b). For both depicted pressure steps, the velocity ratio $u_2/u_{cc} = 1.4$ results in a film-cooling effectiveness $\Theta \approx 0.12$ for an axial position 200 slot heights downstream of the point of injection, independent of the slot heights $s = 0.25$ and 0.4 mm of the film-coolant injection segment.

Results of Figs. 7 and 8 display the importance of the velocity ratio, unlike the coolant injection slot height s, on axial film-cooling effectiveness Θ. The film-cooling effectiveness can be expressed as a function of the film blowing rate, which is mainly a function of the velocity ratio:

$$\Theta\left(\frac{x}{s}\right) = f(M) = f\left(\frac{u_2}{u_{cc}}\right) \tag{10}$$

D. Influence of Injector Geometry

Figure 9 depicts the measured film-cooling effectiveness and the range of circumferential varieties for the angular positions $\xi = 0$ and 18°. The film was injected at the angular positions of the outer coaxial injector elements, located at $\xi = 0$ and 36° in the injector triangle (see Fig. 3).

For all investigated pressure steps (11.5, 8, and 5 MPa) a clear difference in film-cooling effectiveness between a position straight downstream of the slots ($\xi = 0°$) and a position between the film injection slots ($\xi = 18°$) is visible. For a high blowing rate, as depicted in Fig. 9a, the influence of the injector geometry can be

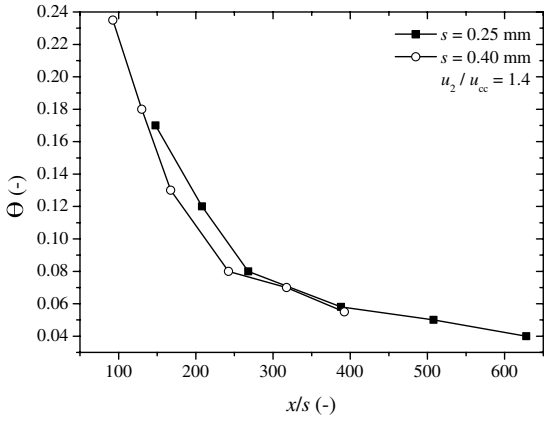

a) p_{cc} = 11.5 MPa

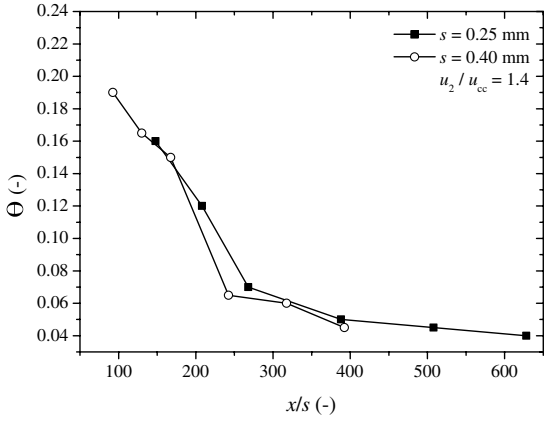

b) p_{cc} = 8 MPa

Fig. 8 Influence of slot height s ($\xi = 18°$).

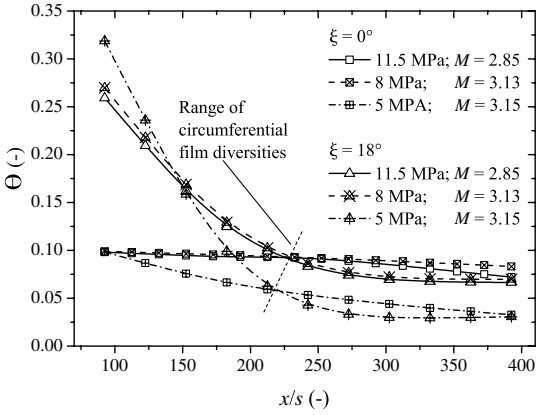

a) High blowing rate M

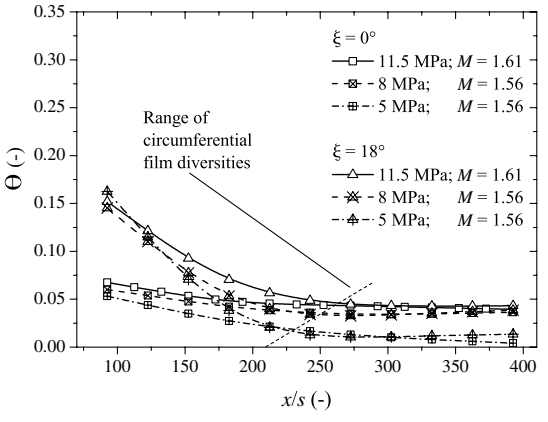

b) Low blowing rate M

Fig. 9 Circumferential film-cooling variety.

neglected downstream of $x/s \approx 220$–240. From this position an evenly distributed film in the circumferential direction can be ensured. Almost the same behavior can be seen for a low film blowing rate (see Fig. 9b). However, a higher combustion-chamber pressure results in a slight downstream shifting of the position where the differences in film effectiveness between $\xi = 0$ and 18° disappear. The investigation shows that almost independent of combustion-chamber pressure and film blowing rate, an equalization of the circumferential film-cooling effectiveness can be detected downstream of a film-cooling length of $x/s \approx 220$–270.

Previous investigations at DLR Lampoldshausen provided evidence that this behavior with a higher film efficiency between the slots can be explained by superposition effects and displacement of the coolant because of a relatively low momentum ratio compared with the injector flow [13,14].

E. Influence of Circumferential Slot Positioning

To investigate the influence of circumferential slot positioning, two different slot configurations applying a constant slot height $s = 0.4$ mm were compared in terms of wall temperature and film-cooling effectiveness. In addition to the standard slot positioning with film injection at the angular positions of the outer coaxial injector elements (slot configuration I), a second configuration II with film injection between the outer injector elements was applied (see Fig. 10). Film injection slots are located at $\xi = 0$ and 36° in the injector triangle for configuration I (see also Fig. 3) and are located at $\xi = -18$, 18, and 54° for configuration II.

Figure 11 depicts the comparison of the film effectiveness using film injection configuration I (Θ_I) and film effectiveness using slot configuration II (Θ_{II}). The influence of the slot positioning on film-cooling effectiveness was investigated for positions downstream of the outer coaxial injector elements at $\xi = 0°$ and for positions between the outer coaxial elements at $\xi = 18°$ in the injector triangle.

Investigations showed a significant increase in film-cooling effectiveness at the position $\xi = 18°$ for film injection using configuration II in comparison with configuration I, especially in close proximity to the film injection point. With increasing film-cooling length x/s an equalization between Θ_I and Θ_{II} can be determined. However, when injecting a film at the angular position $\xi = 0°$ following slot configuration II, a significant reduction of film-cooling effectiveness Θ_{II}, especially close to the injection, was measured. Because of the high momentum of the propellants injected at the position $\xi = 0°$ compared with the low momentum of the injected film at the same angular position with configuration I, a displacement of the film is most likely. This displacement of the film coolant results in a steep reduction of the film effectiveness

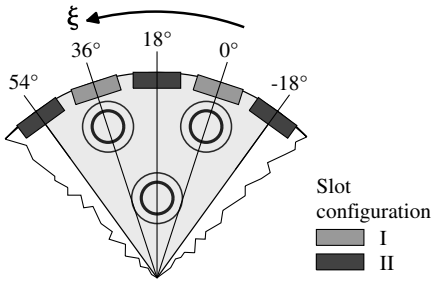

Fig. 10 Slot positioning in the injector triangle.

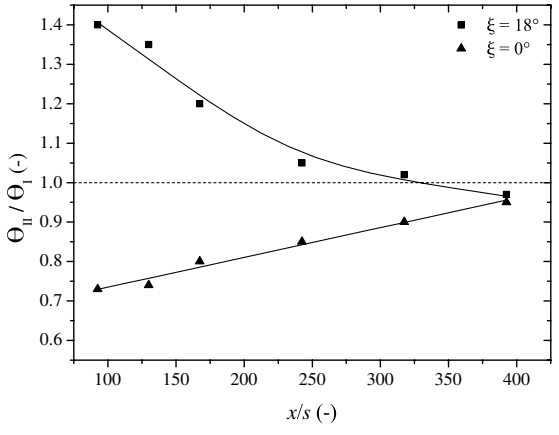

Fig. 11 Influence of slot position.

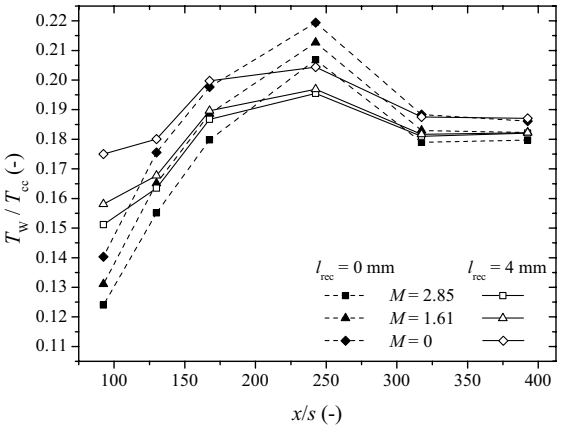

a) p_{cc} = 11.5 MPa

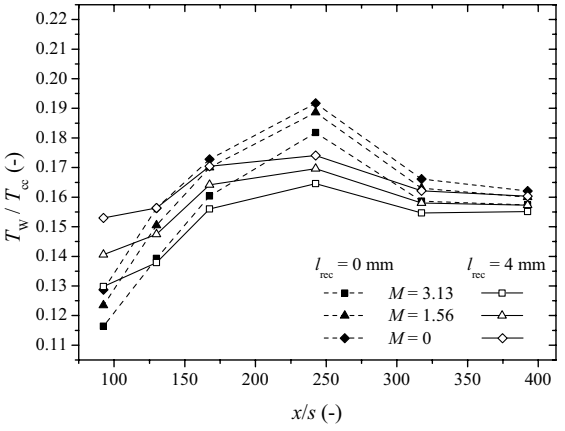

b) p_{cc} = 8 MPa

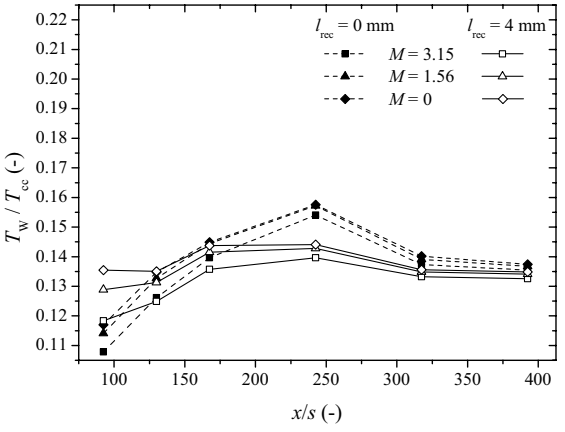

c) p_{cc} = 5 MPa

Fig. 12 Influence of recess ($\xi = 0°$, $s = 0.4$ mm).

Table 5 Reproducibility of hot-gas conditions

Interval	1	2	3	4	5	6	7	8	9
$p_{cc,A}/p_{cc,B}$	0.997	0.996	0.996	0.996	0.996	0.998	0.996	0.996	0.996
ROF_A/ROF_B	0.998	0.996	0.997	0.999	0.997	0.997	0.999	0.998	0.999

Table 6 Reproducibility of measured temperatures

x/s	92.5	130.0	167.5	242.5	317.5	392.5
$T_{W,A}/T_{W,B}$	0.994	0.991	0.991	1.005	0.989	0.992

downstream of the outer coaxial injector elements and film-cooling slots, as depicted in Fig. 9 [13,14]. When the film is injected at the positions between the coaxial injectors, the high propellant momentum hinders an effective cooling at the positions downstream of the injector elements even more. This can cause both a significant increase in thermal load and the requirement of a higher film mass flow rate to compensate for this effect when using slot configuration II.

In terms of a preferably uniform temperature distribution in the circumferential direction, slot configuration I is preferable to minimize circumferential thermal variations in the chamber wall material.

The influence of combustion-chamber pressure and film blowing rate was found to be negligible during the present investigations for the ratio of Θ_{II}/Θ_{I}.

F. Influence of Injector Recess

Figure 12 depicts the comparison of axial wall temperature distribution for two different injector recess lengths: $l_{rec} = 0$ and 4 mm. The influence of the injector recess length is clearly visible for all pressure steps p_{cc} and film-cooling blowing rates M.

A recess length $l_{rec} = 0$ mm results in both comparable low wall temperatures in close proximity of the injector head and in a steep temperature increase with increasing axial distance x/s. The maximum wall temperature is reached approximately 250 film injection slot heights ($s = 0.4$ mm) downstream of the injector-head face plate. Further downstream from this position, the combustion process is completed and a reduction in wall temperature is noticeable. The application of a film injected at position $x/s = 0$ gives a lower wall temperature, especially close to the point of film injection, but is also perceivable at the end of the cylindrical segment.

The axial wall temperature distribution when featuring a recess length $l_{rec} = 4$ mm yields a higher wall temperature T_W close to the injector head. However, the following temperature increase with increasing axial distance is much smoother. The maximum axial wall temperatures were also measured at the position $x/s = 250$, independent of the recess length. The values of the maximum temperatures are significantly reduced due to the application of an injector recess, as depicted in Figs. 12a–12c for the different pressure steps 11.5, 8, and 5 MPa, respectively.

The influence of film cooling ($M > 0$) is visible for all investigated pressure steps. In close proximity of the injector head and film injection point, a recess length $l_{rec} = 4$ mm gives a much more pronounced influence of the injected film than for a recess length $l_{rec} = 0$ mm, as shown in Fig. 12. Farther downstream the wall temperature reduction due to film cooling shows no connection to the injector configuration anymore.

The comparison of the measurements with and without injector recess shows a much more balanced temperature distribution in the case of a recess.

IV. Error Analysis

The absolute accuracy of the measured data is just as important as the reproducibility of the experiment. The heat load inside a rocket combustion chamber is predominantly driven by the combustion-chamber pressure p_{cc} and the propellant mixture ROF. The comparison of two hot runs A und B with identical P8 test bench conditions (see Table 5) shows the excellent reproducibility of the test bench and therefore also the reproducibility of the hot-gas condition inside the combustion chamber.

Comparable results have been achieved with the measured temperatures (see Table 6) for maximum deviation at various axial positions x/s. The deviation of the results of the wall thermocouples is less than 2%. Assuming a hot-gas side-wall temperature of 800 K, the maximum fluctuation range of the local wall temperatures between two hot runs can be estimated with approximately ± 15 K.

Taking into account measurement errors due to the application of thermocouples in the chamber wall, the following estimation can be done to judge the maximum wall thermocouple measurement error as a function of the radial thermal gradient $T_{W1} - T_{W2}$ (see Fig. 13).

Figure 14 depicts the x-ray of two different wall thermocouples. The different arrangement of the thermocouple wires inside the thermocouples and the different formation of the tip is clearly visible. Not only does the application of the thermocouples in the chamber wall have an influence on the measurement error, but so does the manufacturing variation of single thermocouples. A low deviation of arrangement and fabrication of the thermocouple tip is essential for high-accuracy temperature measurements, especially with high-temperature gradients inside the chamber wall material close to the hot-gas side in the range of 100–300 K/mm.

Finally, film-cooling effectiveness errors can be judged with $\Delta\Theta \approx 0.002$–$0.025$ [13,14,18]. In consideration of the large-scale tests with a Vulcain 2-like hot-gas situation, the errors in describing wall temperatures and film cooling in the subscale rocket combustion chamber are small by way of comparison.

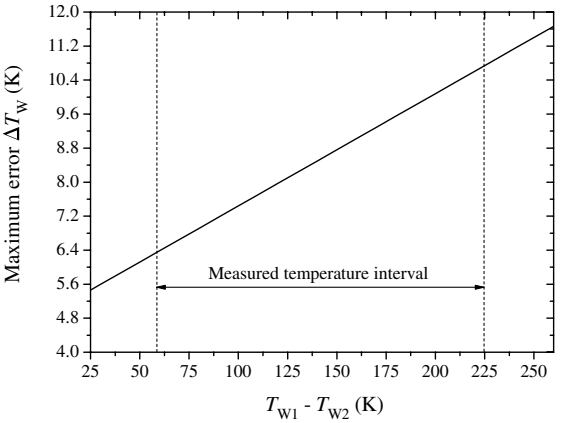

Fig. 13 Wall temperature error.

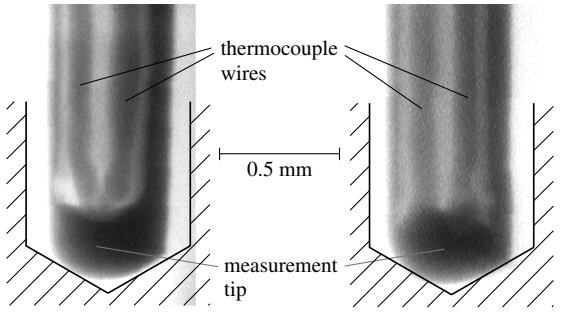

Fig. 14 X-ray photographs of wall thermocouples.

V. Conclusions

The present study gives a detailed overview of a variety of influence parameters on film-cooling effectiveness. Tangential slot injection was investigated for real enginelike conditions with chamber pressures of 5, 8, and 11.5 MPa using a LOX/GH_2 fired subscale combustion chamber. GH_2 with ambient temperatures was applied as a film coolant. The experimental investigations confirmed the dominant influence of the film blowing rate on film-cooling effectiveness. An increase of the film blowing rate results in a direct improvement of the local film-cooling effectiveness. An almost linear relationship between film blowing rate and film-cooling effectiveness was measured downstream of the point of coolant injection. The velocity ratio between film and hot gas as well as the slot Reynolds number are also main parameters for characterizing film-cooling effectiveness. Generally speaking, an increase in slot Reynolds number results in a direct enhancement in film-cooling effectiveness. However, an increase in slot Reynolds number produces higher turbulence effects and higher mixture of secondary and main fluids, which leads to a decrease in film-cooling effectiveness for slot Reynolds numbers exceeding 6.5×10^5. The influence of the film injection slot height s is emphasized to be secondary in the investigated range of slot heights $s = 0.4$ and 0.25 mm, since a change in slot height also results in a different velocity ratio when assuming constant film mass flow rates. By the application of an injector recess, the axial temperature distribution in the cylindrical chamber segment is much smoother than without a recess. The maximum temperature is reduced significantly. The influence of film cooling is more pronounced close to the point of injection when featuring a recess length. The circumferential film injection slot positioning is a significant parameter for a uniform coolant distribution in the chamber. A much more uniform temperature distribution can be reached by film injection at the angular positions of the outer coaxial injector elements instead of an injection between these elements.

Further experimental film-cooling investigations are planned at DLR Lampoldshausen. This includes not only the use of green propellants (LOX/CH_4), but also film cooling in a convectively and film-cooled Vulcain 2-like subscale nozzle [39].

Acknowledgment

The authors would like to thank the P8 team for their assistance.

References

[1] Sutton, G. P., "History of Liquid Propellant Rocket Engines in the United States," *Journal of Propulsion and Power*, Vol. 19, No. 6, 2003, pp. 978–1007. doi:10.2514/2.6942

[2] Sutton, G. P., "History of Liquid-Propellant Rocket Engines in Russia, Formerly the Soviet Union," *Journal of Propulsion and Power*, Vol. 19, No. 6, 2003, pp. 1008–1037. doi:10.2514/2.6943

[3] de Korver, V., Lassoudiere, F., and Fiorentino, C., "Vulcain X Technological Demonstration Roadmap," 42nd AIAA/ASME/SAE/ASEE Joint Propulsion Conference and Exhibit, Sacramento, CA, AIAA Paper 2006-4699, July 2006.

[4] Sutton, G. P., Wagner, W. R., and Seader, J. D., "Advanced Cooling Techniques for Rocket Engines," *Astronautics and Aeronautics*, Vol. 4, Jan. 1966, pp. 60–71.

[5] Huzel, D. K., and Huang, D. H., *Modern Engineering for Design of Liquid-Propellant Rocket Engines*, Vol. 147, Progress in Astronautics and Aeronautics, AIAA, Washington, D.C., 1992.

[6] Terry, J. E., and Caras, G. J., "Transpiration and Film Cooling of Liquid Rocket Nozzles," Redstone Scientific Information Center, TR N 66 38728, U. S. Army Missile Command, Redstone Arsenal, AL, March 1966.

[7] Volkmann, J. C., Tuegel, L. M., and McLeod, J. M., "Gas Side Heat Flux and Film Coolant Investigation for Advanced LOX/Hydrocarbon Thrust Chambers," 26th AIAA/SAE/ASME/ASEE Joint Propulsion Conference, Orlando, FL, AIAA Paper 90-2184, July 1990.

[8] Volkmann, J. C., McLeod, J. M., and Claflin, S. E., "Investigation of Throat Film Coolant for Advanced LOX/RP-1 Thrust Chambers," 27th AIAA/SAE/ASME/ASEE Joint Propulsion Conference, Sacramento, CA, AIAA Paper 91-1979, June 1991.

[9] Goldstein, R. J., "Film Cooling," *Advances in Heat Transfer*, Vol. 7, 1971, pp. 321–379.

[10] Ligrani, P. M., Ciriello, S., and Bishop, D. T., "Heat Transfer, Adiabatic Effectiveness, and Injectant Distributions of a Single Row and Two Staggered Rows of Compound Angle Film-Cooling Holes," *Journal of Turbomachinery*, Vol. 114, 1992, pp. 687–700. doi:10.1115/1.2928021

[11] Honami, S., Shizawa, T., and Uchiyama, A., "Behaviour of the Laterally Injected Jet in Film Cooling: Measurements of Surface Temperature and Velocity/Temperature Field Within the Jet," *Journal of Turbomachinery*, Vol. 116, 1994, pp. 106–112. doi:10.1115/1.2928264

[12] Ekkad, S. V., Zapata, D., and Han, J.-C., "Film Effectiveness over a Flat Plate Surface with Air and CO_2 Injection Through Compound Angle Holes Using a Transient Liquid Crystal Image Method," ASME Turbo Expo, Houston, TX, ASME Paper 95-GT-11, June 1995.

[13] Arnold, R., Suslov, D., and Haidn, O. J., "Influence Parameters on Film Cooling Effectiveness in a High Pressure Subscale Combustion Chamber," 47th AIAA Aerospace Sciences Meeting, Orlando, FL, AIAA Paper 2009-0453, Jan. 2009.

[14] Arnold, R., Suslov, D., and Haidn, O. J., "Circumferential Film Cooling Effectiveness in a LOX/H_2 Subscale Combustion Chamber," *Journal of Propulsion and Power*, Vol. 25, No. 3, May–June 2009, pp. 760–770. doi:10.2514/1.40305

[15] Arnold, R., Suslov, D., and Haidn, O. J., "Film Cooling of Accelerated Flow in a Subscale Combustion Chamber," *Journal of Propulsion and Power*, Vol. 25, No. 2, March–April 2009, pp. 443–451. doi:10.2514/1.39308

[16] Arnold, R., Suslov, D., Weigand, B., and Haidn, O. J., "Investigation of Film Cooling in a High Pressure LOX/GH_2 Subscale Combustion Chamber," Space Propulsion 2008: 5th International Spacecraft Propulsion Conference, Heraklion, Crete, Greece, Paper 42 090, May 2008.

[17] Arnold, R., Suslov, D. I., and Haidn, O. J., "Experimental Investigation of Film Cooling with Tangential Slot Injection in a LOX/CH_4 Subscale Rocket Combustion Chamber," *Transactions of JSASS, Space Technology Japan*, Vol. 7, Japan Society for Aeronautical and Space Sciences, Tokyo, 2009, pp. Pa_81–Pa–86. doi:10.2322/tstj.7.Pa_81

[18] Arnold, R., "Experimentelle Untersuchungen zur Filmkühlung in Raketenbrennkammern," Ph.D. Thesis, Universität Stuttgart, Stuttgart, Germany, Dec. 2008.

[19] Eckert, E. R. G., and Birkebak, R. C., "The Effects of Slot Geometry on Film Cooling," *Heat Transfer, Thermodynamics, and Education*, McGraw–Hill, edited by H. A. Johnson, New York, 1964, pp. 150–163.

[20] Stollery, J. L., and El-Ehwany, A. A. M., "A Note on the Use of a Boundary-Layer Model for Correlating Film-Cooling Data," *International Journal of Heat and Mass Transfer*, Vol. 8, 1965, pp. 55–65. doi:10.1016/0017-9310(65)90097-9

[21] Burns, W. K., and Stollery, J. L., "The Influence of Foreign Gas Injection and Slot Geometry on Film Cooling Effectiveness," *International Journal of Heat and Mass Transfer*, Vol. 12, 1969, pp. 935–951. doi:10.1016/0017-9310(69)90156-2

[22] Fröhlke, K., Haberzettl, A., Haidn, O. J., Heinrich, S., Sion, M., and Vuillermoz, P., "First Hot Fire Test Campaign at the French-German Research Facility P8," 33rd AIAA/ASME/SAE/ASEE Joint Propulsion Conference and Exhibit, Seattle, WA, AIAA Paper 97-2929, July 1997.

[23] Koschel, W. W., Haidn, O. J., and Krülle, G., "P8-The New French/German Test Facility for H_2/O_2-High Pressure Rocket Engine Combustion Research," *International Journal of Hydrogen Energy*, Vol. 23, No. 8, 1998, pp. 1815–1825.

[24] Arnold, R., Suslov, D., Weigand, B., and Haidn, O. J., "Circumferential Behavior of Tangential Film Cooling and Injector Wall Compatibility in a High Pressure LOX/GH_2 Subscale Combustion Chamber," 44th AIAA/ASME/SAE/ASEE Joint Propulsion Conference and Exhibit, Hartford, CT, July 2008, AIAA Paper 2008-5242.

[25] Kays, W., Crawford, M. E., and Weigand, B., *Convective Heat and Mass Transfer*, 4th ed.,McGraw–Hill, New York, 2005.

[26] Suslov, D., Woschnak, A., Sender, J., and Oschwald, M., "Test Specimen Design and Measurement Technique for Investigation of Heat Transfer Processes in Cooling Channels of Rocket Engines under Real Thermal Conditions," 24th International Symposium on Space Technology and Science (ISTS), Miyazaki, Japan, ISTS Paper 2004-e-40, May 2004.

[27] Suslov, D., Woschnak, A., Greuel, D., and Oschwald, M., "Measurement Techniques for Investigation of Heat Transfer Processes at European Research and Technology Test Facility P8," *European*

Conference for Aerospace Sciences (EUCASS), Moscow, July 2005.

[28] Oschwald, M., Suslov, D., and Woschnak, A., "Einfluss der Temperaturabhängigkeit der Materialeigenschaften auf den Wärmehaushalt in Regenerativ Gekühlten Brennkammern," *Deutscher Luftund Raum-Fahrtkongress*, Paper DGLR-2004/111, Dresden, Germany, Sept. 2004.

[29] Goldstein, R. J., Eckert, E. R. G., Tsou, F. K., and Haji-Sheikh, A., "Film Cooling with Air and Helium Injection Through a Rearward-Facing Slot into a Supersonic Air Flow," *AIAA Journal*, Vol. 4, No. 6, June 1966, pp. 981–985. doi:10.2514/3.3591

[30] Goldstein, R. J., Rask, R. B., and Eckert, E. R. G., "Film Cooling with Helium Injection into an Incompressible Air Flow," *International Journal of Heat and Mass Transfer*, Vol. 9, 1966, pp. 1341–1350. doi:10.1016/0017-9310(66)90132-3

[31] Papell, S., and Trout, A. M., "Experimental Investigation of Air Film Cooling Applied to an Adiabatic Wall by Means of an Axially Discharging Slot," NASA TR TN D-9, Aug. 1959.

[32] Lucas, J. G., and Golladay, R. L., "An Experimental Investigation of Gaseous Film Cooling of a Rocket Motor," NASA TR TN D-1988, Oct. 1963.

[33] Goldstein, R. J., and Haji-Sheikh, A., "Prediction of Film Cooling Effectiveness," JSME 1967 Semi-International Symposium, Tokyo, Japan, Paper 225, Sept. 1967.

[34] Goldstein, R. J., Eckert, E. R. G., and Wilson, D. J., "Film Cooling with Normal Injection into a Supersonic Flow," *Journal of Engineering for Industry*, Vol. 90, No. 4, Nov. 1968, pp. 584–588.

[35] Goldstein, R. J., Eckert, E. R. G., Eriksen, V. L., and Ramsey, J. W., "Film Cooling Following Injection Through Inclined Circular Holes," *Israel Journal of Technology*, Vol. 8, No. 1–2, March 1970, pp. 145–154.

[36] Goldstein, R. J., and Stone, L. D., "Row-of-Holes Film Cooling of Curved Walls at Low Injection Angles," *Journal of Turbomachinery*, Vol. 119, 1997, pp. 574–579.

[37] Goldstein, R. J., and Jin, P., "Film Cooling Downstream of a Row of Discrete Holes with Compound Angle," *Journal of Turbomachinery*, Vol. 123, April 2001, pp. 222–230. doi:10.1115/1.1344905

[38] Papell, S., "Effect on Gaseous Film Cooling of Coolant Injection Through Angled Slots and Normal Holes," NASA TR TN D-299, Sept. 1960.

[39] Suslov, D. I., Arnold, R., and Haidn, O. J., "Convective and Film-Cooled Nozzle Extension for a High Pressure Rocket Subscale Combustion Chamber," 48th AIAA Aerospace Sciences Meeting, Orlando, FL, AIAA Paper 2010-1150, Jan. 2010.

K. Frendi
Associate Editor